Ab Initio and Experimental Studies on the Structure and Relative Stability of the *cis*-Hydride−η^2-Dihydrogen Complexes $[\{P(CH_2CH_2PPh_2)_3\}M(H)(\eta^2\text{-}H_2)]^+$ (M = Fe, Ru)

Claudio Bianchini,* Dante Masi, and Maurizio Peruzzini

Istituto per lo Studio della Stereochimica ed Energetica dei Composti di Coordinazione del CNR, Via J. Nardi 39, 50132, Firenze, Italy

Maurizio Casarin,* Chiara Maccato, and Gian Andrea Rizzi

Dipartimento di Chimica Inorganica, Metallorganica ed Analitica, Università di Padova, Via Loredan 4-35131, Padova, Italy

Received June 14, 1996[⊗]

Ab initio calculations (DMOL method) including the estimate of the total energy and the full optimization of the geometrical parameters have been used to study the electronic structures and the coordination geometries of the model systems $[\{P(CH_2CH_2PH_2)_3\}M(H)(L)]^+$ (M = Fe, L = H_2, C_2H_4, CO, N_2; M = Ru, L = H_2). Single crystal X-ray analyses have been carried out on the complexes $[(PP_3)Fe(H)(\eta^2\text{-}H_2)]BPh_4\cdot 0.5THF$ (**1**·0.5THF), $[(PP_3)Fe(H)(CO)]BPh_4\cdot THF$ (**3**·THF), and $[(PP_3)Ru(H)(\eta^2\text{-}H_2)]BPh_4\cdot 0.5THF$ (**5**·0.5THF) [$PP_3 = P(CH_2CH_2PPh_2)_3$]. Crystal data: for **1**·0.5THF, *triclinic P*1 (No. 2), $a = 17.626(3)$ Å, $b = 14.605(3)$ Å, $c = 12.824(4)$ Å, $\alpha = 90.09(2)°$, $\beta = 103.87(2)°$, $\gamma = 107.46(2)°$, $Z = 2$, $R = 0.082$; for **3**·THF, *triclinic P*1 (No. 2), $a = 12.717(2)$ Å, $b = 14.553(1)$ Å, $c = 17.816(2)$ Å, $\alpha = 72.90(1)°$, $\beta = 76.82(2)°$, $\gamma = 89.71(1)°$, $Z = 2$, $R = 0.067$; for **5**·0.5THF, *monoclinic P*2/1*a* (No. 14), $a = 19.490(5)$ Å, $b = 19.438(2)$ Å, $c = 16.873(5)$ Å, $\beta = 110.96(2)°$, $Z = 4$, $R = 0.074$. On the basis of theoretical calculations, X-ray analyses, and multinuclear NMR studies, all of the complexes of the formula $[(PP_3)M(H)(L)]BPh_4$ [M = Fe, L = H_2 (**1**), C_2H_4 (**2**), CO (**3**), N_2 (**4**); M = Ru, L = H_2 (**5**), C_2H_4 (**6**)] are assigned a distorted octahedral structure where the hydride (trans to a terminal phosphorus donor) and the L ligand occupy mutually cis positions. The theoretical calculations indicate that the H_2 ligand in the η^2-dihydrogen−hydride derivatives **1** and **5** is placed in the P−M−H plane (parallel orientation) and that there is an attractive interaction between the H and H_2 ligands. XPS measurements, performed on the iron complexes, show that the Fe → L back-bonding interaction plays a leading role in **3**. It is concluded that the stronger metal−H_2 bond in the dihydrogen−hydride complex **1**, as compared to the Ru analog **5**, is due to the greater *d*(metal) → σ^*(H−H) back-donation as well as a more efficient interaction between the terminal hydride and an H of the dihydrogen ligand. This cis effect is suggested to contribute to the relative stability of the iron complexes, which increases in the order $C_2H_4 < N_2 < H_2 < CO$.

Introduction

The different strength of the M−H_2 bond is the key factor which controls and distinguishes the varied chemistry of the two *cis*-hydride−η^2-dihydrogen complexes $[(PP_3)M(H)(\eta^2\text{-}H_2)]BPh_4$ [M = Fe, **1**; Ru, **5**; $PP_3 = P(CH_2CH_2PPh_2)_3$].[1,2]

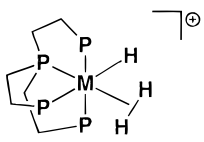

M = Fe, **1**; Ru, **5**

The dihydrogen ligand is so strongly bound to the iron center that when **1** is employed as a homogeneous catalyst for the hydrogenation of 1-alkynes to alkenes, a free coordination site for the incoming alkyne molecule is provided by detachment of a phosphine arm, rather than by H_2 loss.[3] In contrast, the hydrogenation of 1-alkynes catalyzed by **5** occurs, as is usually observed in analogous reactions,[4] by initial displacement of H_2 by the substrate.[5] Similarly, the use of either **1** or **5** as catalyst precursors for the hydrogen-transfer reductions of α,β-unsaturated ketones results in distinct activities and chemoselectivities just because of the stronger metal−H_2 bond in the iron derivative.[6]

[⊗] Abstract published in *Advance ACS Abstracts,* February 1, 1997.

(1) (a) Bianchini, C.; Peruzzini, M.; Zanobini, F. *J. Organomet. Chem.* **1988**, *354*, C19. (b) Bianchini, C.; Peruzzini, M.; Polo, A.; Vacca, A.; Zanobini, F. *Gazz. Chim. Ital.* **1991**, *121*, 543.

(2) Bianchini, C.; Perez, P. J.; Peruzzini, M.; Zanobini, F.; Vacca, A. *Inorg. Chem.* **1991**, *30*, 279.

(3) (a) Bianchini, C.; Meli, A.; Peruzzini, M.; Frediani, P.; Bohanna, C.; Esteruelas, M. A.; Oro, L. A. *Organometallics* **1992**, *11*, 138. (b) Bianchini, C.; Meli, A.; Peruzzini, M.; Frediani, P.; Bohanna, C.; Esteruelas, M. A.; Oro, L. A. In *Advances in Catalyst Design*; Graziani, M., Rao, C. N. R., Eds.; World Scientific: Singapore, 1991; p 267. (c) Bianchini, C.; Meli, A.; Peruzzini, M.; Vizza, F.; Zanobini, F. *Organometallics* **1989**, *8*, 2080.

(4) See for example: (a) Andriollo, A.; Esteruelas, M. A.; Meyer, U.; Oro, L. A.; Sánchez-Delgado, R. A.; Sola, E.; Valero, C.; Werner, H. *J. Am. Chem. Soc.* **1989**, *111*, 7431. (b) Albertin, G.; Amendola, P.; Antoniutti, S.; Ianelli, S.; Pelizzi, G.; Bordignon, E. *Organometallics* **1991**, *10*, 2876. (c) Marinelli, G.; Rachidi, I. E.-I.; Streib, W. E.; Eisenstein, O.; Caulton, K. G. *J. Am. Chem. Soc.* **1989**, *111*, 2346. (d) Christ, M. L.; Sabo-Etienne, S.; Chaudret, B. *Organometallics* **1995**, *14*, 1082. (e) Esteruelas, M. A.; Herrero, J.; Lòpez, A. M.; Oro, L. A.; Schulz, M.; Werner, H. *Inorg. Chem.* **1982**, *31*, 4013. (f) Esteruelas, M. A.; Oro, L. A.; Valero, C. *Organometallics* **1992**, *11*, 3362. (g) Espuelas, M. A.; Esteruelas, M. A.; Lahoz, F. J.; Oro, L. A.; Valero, C. *Organometallics* **1993**, *12*, 663. (h) Harman, W. D.; Taube, H. *J. Am. Chem. Soc.* **1990**, *112*, 2261. (i) Lin, Y. R.; Zhou, Y. F. *J. Organomet. Chem.* **1990**, *381*, 135. (j) Bianchini, C.; Farnetti, E.; Frediani, P.; Graziani, M.; Peruzzini, M.; Polo, A. *J. Chem. Soc., Chem. Commun.* **1991**, 1336.

(5) Bianchini, C.; Bohanna, C.; Esteruelas, M. A.; Frediani, P.; Meli, A.; Oro, L. A.; Peruzzini, M. *Organometallics* **1992**, *11*, 3837.

S0020-1669(96)00736-7 CCC: $14.00

In an initial attempt to rationalize the different metal−dihydrogen bond strength in **1** and **5**, the barrier to rotation of the H_2 ligand was determined from inelastic neutron scattering (INS) studies of the H_2 rotational energy levels.[7] From this investigation, it was concluded that the Fe center (rotational barrier of 1.82 kcal mol^{-1}) is a better back-donor than Ru (rotational barrier of 1.36 kcal mol^{-1}).[8] Analogous conclusions were also reached by Morris and co-workers from NMR studies on isostructural η^2-H_2 complexes of the Fe group (Fe, Ru, Os).[9,10] Back-donation arguments alone, however, cannot explain the differences in the reactions of the two compounds in solution. In particular, they do not account for the fact that H_2 readily displaces the ethene ligand from $[(PP_3)Fe(H)(C_2H_4)]BPh_4$ in which the back-bonding contribution is greater than in **1**, whereas H_2 does not displace ethene from $[(PP_3)Ru(H)(C_2H_4)]BPh_4$ (*vide infra*). In other words, the extraordinarily strong binding of the H_2 ligand to iron may not be only a function of the donation [M ← $\sigma(H_2)$] and back-donation [M → $\sigma^*(H_2)$] contributions.[11,12] The so called "cis effect",[13] the attractive two-electron interaction between cis σ(M−H) and σ^*(H−H), might play a key role in determining the overall stability of the present *cis*-hydride−η^2-dihydrogen Fe and Ru complexes. The cis effect, in fact, not only may control the orientation of the H_2 ligand in nonclassical polyhydrides[13,14] but also may influence the strength of the metal−dihydrogen bond,[14] as shown by *ab initio* MO calculations in the related model system *cis*-$[Fe(PH_3)_4(H)(H_2)]^+$.[14,15]

In a further attempt to gain insight into the different chemistry of **1** and **5**, the solid-state structures of both compounds were determined by X-ray diffraction analyses. The crystallographic results, which are presented in this paper, however, do not allow one to discuss the relative orientation of the H and H_2 ligands as the dihydrogen ligands could not satisfactorily be located. Thus, we decided to perform a theoretical analysis of the prototype complex cations $[\{P(CH_2CH_2PH_2)_3\}M(H)(H_2)]^+$ (M = Fe, **1***; M = Ru, **5***) through calculations which include the estimate of the total energy and the full optimization of the geometrical parameters. The theoretical analysis has been extended to other members of the iron family, namely, the cations $[\{P(CH_2CH_2PH_2)_3\}Fe(H)(L)]^+$ (L = C_2H_4, **2***; CO, **3***; N_2, **4***), with the aim of understanding the trend in the qualitative stability of the actual compounds $[(PP_3)Fe(H)(L)]BPh_4$ (L = H_2, CO, C_2H_4, N_2)[1,16] with respect to the dissociation of the L ligand, which increases in the order $C_2H_4 < N_2 < H_2 < CO$. Within this context, valuable information has been provided by XPS measurements carried out on all of the iron complexes.

The experimental and theoretical studies, taken together, provide a concerted view of the molecular structure of **1** and **5** and the difference in their chemistry.

Experimental Section

Reagents. Tetrahydrofuran (THF) was purified by distillation under nitrogen over $LiAlH_4$. All of the other reagents and chemicals were reagent grade and, unless otherwise stated, were used as received by commercial suppliers. All reactions and manipulations were routinely performed under a dry argon atmosphere by using standard Schlenk-tube techniques. The solid complexes were collected on sintered glass frits and washed with light petroleum ether (bp 40−60 °C) or *n*-pentane before being dried in a stream of argon. The ligand $P(CH_2CH_2PPh_2)_3$ (PP_3) was purchased from Pressure Co. and used without further purification. The complexes $[(PP_3)Fe(H)(\eta^2\text{-}H_2)]BPh_4$ (**1**),[1] $[(PP_3)Fe(H)(\eta^1\text{-}N_2)]BPh_4$ (**4**),[1] $[(PP_3)Ru(H)(\eta^2\text{-}H_2)]BPh_4$ (**5**),[2] $[(PP_3)Ru(H)(CO)]BPh_4$ (**7**),[2] $[(PP_3)Ru(H)(\eta^1\text{-}N_2)]BPh_4$ (**8**),[2] $[(PP_3)FeH_2]$ (**9**),[17] and $[(PP_3)RuH_2]$ (**10**)[2] were prepared as described in the literature. Elemental analyses (C, H, N) were performed using a Carlo Erba Model 1106 elemental analyzer.

Spectroscopic Measurements. Deuterated solvents for NMR measurements (Merck and Aldrich) were dried over molecular sieves (4 Å). ^{1}H and ^{13}C{^{1}H} NMR spectra were recorded on Varian VXR 300 or Bruker AC200 spectrometers operating at 299.94 or 200.13 MHz (^{1}H) and 75.42 or 50.32 MHz (^{13}C), respectively. Peak positions are relative to tetramethylsilane and were calibrated against the residual solvent resonance (^{1}H) or against the deuterated solvent multiplet (^{13}C). ^{13}C-DEPT experiments were run on the Bruker AC200 spectrometer. The ^{1}H,^{13}C-2D HETCOR NMR experiment on complex **6** was recorded on a Bruker AVANCE DRX 500 spectrometer equipped with a 5-mm triple resonance probe head for ^{1}H detection and inverse detection of the heteronucleus (inverse correlation mode, HMQC experiment) with no sample spinning. ^{31}P{^{1}H} NMR spectra were recorded on either the Varian VXR 300 or Bruker AC200 instruments operating at 121.42 and 81.01 MHz, respectively. Chemical shifts were measured relative to external 85% H_3PO_4 with downfield values taken as positive. Computer simulations of the ^{31}P{^{1}H} NMR spectrum of **6** was carried out with a locally developed package containing the programs LAOCN3[18] and DAVINS[19] run on a Compaq Deskpro 386/25 personal computer. The initial choices of shifts and coupling constants were refined by iterative least-squares calculations using the experimental digitized spectrum. The final parameters gave a satisfactory fit between experimental and calculated spectra, the agreement factor *R* being less than 1% in all cases. Infrared spectra (400−4000 cm^{-1}) were recorded as Nujol mulls on a Perkin-Elmer 1600 Series FT-IR spectrometer between KBr plates.

Preparation of $[(PP_3)Fe(H)(\eta^2\text{-}C_2H_4)]BPh_4$ (2). Method A. Neat $MeOSO_2CF_3$ (65 μL, 0.57 mmol) was syringed into a well-stirred THF (15 mL) suspension of $[(PP_3)FeH_2]$ (**9**) (365 mg, 0.50 mmol) under an atmosphere of dry ethene. Immediately the starting dihydride dissolved to yield a yellow solution. Stirring was continued for 1 h, and then solid $NaBPh_4$ (400 mg, 1.17 mmol) and ethanol saturated with ethene (20 mL) were added. Slow concentration under a steady stream of ethene afforded **2** as yellow microcrystals; yield, 87%.

Method B. Complex **2** was also prepared by bubbling ethene into a THF solution (15 mL) of $[(PP_3)Fe(H)(\eta^1\text{-}N_2)]BPh_4$ (**4**) (200 mg, 0.16 mmol) for 4 h at 0 °C. Addition of ethanol (20 mL) and workup as above gave **2** in 76% yield. Anal. Calcd for $C_{68}H_{67}BFeP_4$: C, 75.99; H, 6.28. Found: C, 75.63; H, 6.36. IR: ν(Fe−H) not observed.

(6) Bianchini, C.; Farnetti, E.; Graziani, M.; Peruzzini, M.; Polo, A. *Organometallics* **1993**, *12*, 3753.
(7) For a general review of INS techniques see: Eckert, J. *Spectrochim. Acta* **1992**, *29*, 747.
(8) Eckert, J.; Albinati, A.; White, R. P.; Bianchini, C.; Peruzzini, M. *Inorg. Chem.* **1992**, *31*, 4241.
(9) Eckert, J.; Blank, H.; Bautista, M. T.; Morris, R. H. *Inorg. Chem.* **1990**, *29*, 747.
(10) (a) Bautista, M. T.; Cappellani, E. P.; Drouin, S. D.; Morris, R. H.; Schweitzer, C. T.; Sella, A.; Zubkowski, J. *J. Am. Chem. Soc.* **1991**, *113*, 4876. (b) Cappellani, E. P.; Drouin, S. D.; Jia, G.; Maltby, P. A.; Morris, R. H. *J. Am. Chem. Soc.* **1994**, *116*, 3375.
(11) General reviews on molecular hydrogen complexes include: (a) Jessop, P. G.; Morris, R. H. *Coord. Chem. Rev.* **1992**, *121*, 155. (b) Kubas, G. J. *Acc. Chem. Res.* **1988**, *21*, 120. (c) Kubas, G. J. *Comments Inorg. Chem.* **1988**, *7*, 17. (d) Crabtree, R. H.; Hamilton, D. G. *Adv. Organomet. Chem.* **1988**, *28*, 299. (e) Heinekey, D. M.; Oldham, W. J., Jr. *Chem. Rev.* **1993**, *93*, 913.
(12) A review on the theoretical work on nonclassical transition metal polyhydrides has appeared: Lin, Z.; Hall, M. B. *Coord. Chem. Rev.* **1994**, *135/136*, 845.
(13) (a) Jackson, S. A.; Eisenstein, O. *Inorg. Chem.* **1990**, *29*, 3910. (b) Riehl, J.-F.; Pélissier, M.; Eisenstein, O. *Inorg. Chem.* **1992**, *31*, 3344. (c) Riehl, J.-F.; Jackson, S. A.; Pélissier, M.; Eisenstein, O. *Bull. Soc. Chim. Fr.* **1992**, *129*, 221. (d) van der Sluys, L. S.; Eckert, J.; Eisenstein, O.; Hall, J. H.; Huffmann, J. C.; Jackson, S. A.; Koetzle, T. F.; Kubas, G. J.; Vergamini, P. J.; Caulton, K. G. *J. Am. Chem. Soc.* **1990**, *112*, 4831.
(14) Maseras, F.; Duran, M.; Lledós, A.; Bertran, J. *J. Am. Chem. Soc.* **1992**, *114*, 2922.
(15) Maseras, F.; Duran, M.; Lledós, A.; Bertran, J. *J. Am. Chem. Soc.* **1991**, *113*, 2879.
(16) Stoppioni, P.; Mani, F.; Sacconi, L. *Inorg. Chim. Acta* **1974**, *11*, 227.
(17) Bianchini, C.; Laschi, F.; Peruzzini, M.; Ottaviani, M. F.; Vacca, A.; Vizza, F.; Zanello, P. *Inorg. Chem.* **1990**, *29*, 3394.
(18) Castellano, S.; Bothner-By, A. A. *J. Chem. Phys.* **1964**, *41*, 3863.
(19) Stephenson, D. S.; Binsch, G. *J. Magn. Reson.* **1980**, *37*, 295.

Table 1. Summary of Crystal Data for **1**·0.5THF, **3**·THF, and **5**·0.5THF

	1·0.5THF	**3**·THF	**5**·0.5THF
chem formula	$C_{68}H_{69}BFeO_{0.5}P_4$	$C_{71}H_{71}BO_2P_4Fe$	$C_{68}H_{69}BRuO_{0.5}P_4$
fw	1084.85	1146.90	1127.21
space group	*P*1 (No. 2)	*P*1 (No. 2)	*P*2/1*a* (No. 14)
a, Å	17.626(3)	12.717(2)	19.490(5)
b, Å	14.605(3)	14.553(1)	19.438(2)
c, Å	12.824(4)	17.816(2)	16.873(5)
α, deg	90.09(2)	72.90(1)	90
β, deg	103.87(2)	76.82(2)	110.96(2)
γ, deg	107.46(2)	89.71(1)	90
V, Å^3	3047.69	3058.86	5969.31
Z	2	2	4
ρ(calcd), g cm^{-3}	1.18	1.24	1.26
radiation	graphite monochromated Cu Kα, $\lambda = 1.5418$ Å	graphite monochromated Mo Kα, $\lambda = 0.710\,69$ Å	graphite monochromated Cu Kα, $\lambda = 1.5418$ Å
μ, cm^{-1}	32.85	3.91	34.96
R^a	0.082	0.067	0.074
$R_w{}^b$	0.087	0.069	0.079

^{a} $R = \sum||F_o| - |F_c||/|F_c|$. ^{b} $R_w = [\sum w(|F_o| - |F_c|)^2/\sum w(F_o)^2]^{1/2}$.

$^{31}P\{^1H\}$ NMR ($C_2D_4Cl_2/C_7D_8$ [2:1 v/v], 121.42 MHz, sealed NMR tube prepared under C_2H_4): at +25 °C, broad AMQ_2 spin system, δ_A 162.0 (br), δ_M 79.7 (br), δ_Q 70.8 (br); at −25 °C, AMQ_2 spin system, δ_A 161.71 (dt, $J_{AM} = 44.4$ Hz, $J_{AQ} = 22.6$ Hz), δ_M 79.45 (dt, $J_{MQ} = 15.4$ Hz), δ_Q 70.38 (dd). ^1H NMR (−25 °C, CD_2Cl_2, 299.94 MHz, sealed NMR tube prepared under C_2H_4): $\delta_{C_2H_4}$ 3.43 (br q, $J_{HP} = 3.0$ Hz, 4H), δ_{FeH} −8.43 (dt, $J_{HPM} = 63.4$ Hz, $J_{HPQ} = 47.7$ Hz, J_{HPA} not resolved ≤ 1 Hz, 1H). The ^{31}P and ^1H spectra did not change down to −80 °C.

Preparation of [(PP$_3$)Fe(H)(CO)]BPh$_4$ (3). This compound was prepared several years ago by Sacconi *et al.* by treatment of a suspension of [(PP$_3$)FeBr]BPh$_4$ in benzene with solid NaBH$_4$ under CO.[16] However, this method gives a moderate yield of **3**. The new procedures described below provide much better yields.

Method A. The hydride−carbonyl complex **3** was prepared by substituting CO for ethene in the above described reaction of **9** with methyl triflate. Upon addition of NaBPh$_4$ and ethanol, the pale yellow solution was concentrated under a stream of argon until lemon yellow crystals of **3** precipitated; yield, 90%.

Method B. Bubbling carbon monoxide into a THF solution of **4** for 15 min at room temperature, followed by workup as described above, gave **3** in 92% yield. Anal. Calcd for $C_{67}H_{63}BFeOP_4$: C, 74.87; H, 5.99. Found: C, 74.79; H, 6.06. IR: ν(Fe−H) 1890 cm^{-1} (m); ν(C≡O) 1927 cm^{-1} (vs). $^{31}P\{^1H\}$ NMR (22 °C, CD_3COCD_3, 121.42 MHz) AMQ_2 spin system: δ_A 169.34 (td, $J_{AM} = 32.3$ Hz, $J_{AQ} = 27.2$ Hz), δ_M 85.85 (dt, $J_{MQ} = 12.0$ Hz), δ_Q 87.64 (dd). ^1H NMR (22 °C, CD_3COCD_3, 299.94 MHz) δ_{FeH} −12.78 (tdd, $J_{HPQ} = 59.4$ Hz, $J_{HPM} = 48.9$ Hz, $J_{HPA} = 17.7$ Hz, 1H).

Preparation of [(PP$_3$)Ru(H)(η^2-C$_2$H$_4$)]BPh$_4$ (6). Method A. Neat $MeOSO_2CF_3$ (65 μL, 0.57 mmol) was syringed into a well-stirred THF (15 mL) suspension of [(PP$_3$)RuH$_2$] (**10**) (400 mg, 0.52 mmol) under an atmosphere of prepurified ethene. Immediately the starting dihydride dissolved to yield a colorless solution. Stirring was continued for 1 h, and then solid NaBPh$_4$ (400 mg, 1.17 mmol) and ethanol saturated with ethene (20 mL) were added. Slow concentration under a steady stream of ethene afforded **6** as off-white microcrystals; yield 90%.

Method B. The (hydride)ethene complex **6** was prepared by bubbling ethene into a THF solution (10 mL) of either [(PP$_3$)Ru(H)-(η^2-H$_2$)]BPh$_4$ (**5**) (200 mg, 0.18 mmol) or [(PP$_3$)Ru(H)(η^1-N$_2$)]BPh$_4$ (**8**) (200 mg, 0.16 mmol) for 30 min at room temperature. Upon addition of ethanol (20 mL) and concentration under ethene, off-white crystals of **6** precipitated; yield 90%. Anal. Calcd for $C_{68}H_{67}BRuP_4$: C, 72.92; H, 6.03. Found: C, 72.84; H, 5.95. IR: ν(Ru−H) 1972 cm^{-1} (w br). $^{31}P\{^1H\}$ NMR (20 °C, CD_2Cl_2, 121.42 MHz), AMN_2 spin system: δ_A 144.16 (dt, $J_{AM} = 19.5$ Hz, $J_{AN} = 10.5$ Hz), δ_M 55.51, δ_Q 54.86 (second order MN_2 multiplet, $J_{MN} = 13.0$ Hz). ^1H NMR (20 °C, CD_2Cl_2, 299.94 MHz) δ_{C2H4} 3.58 (br s, H), δ_{RuH} −8.85 (dtd, $J_{HPA} = 20.1$ Hz, $J_{HPM} = 48.3$ Hz, $J_{HPN} = 20.9$ Hz, 1H). $^{13}C\{^1H\}$ NMR (20 °C, CD_2Cl_2, 75.45 MHz): $\delta_{C_2H_4}$ 51.69 (dq, $J_{CPA} = 7.5$ Hz, $J_{CPM} \approx J_{CPN} = 1.3$ Hz).

X-ray Diffraction Studies. A summary of crystal and intensity data for the compounds **1**·0.5C_4H_8O, **3**·C_4H_8O, and **5**·0.5C_4H_8O are summarized in Table 1. Experimental data were recorded at room temperature on either an Enraf-Nonius CAD4 diffractometer (**3**·C_4H_8O) or a Philips-PW1100 diffractometer (**1**·0.5C_4H_8O and **5**·0.5C_4H_8O) with an upgraded computer control (FEBO system) using graphite-monochromated Mo Kα radiation (**3**·C_4H_8O) or graphite-monochromated Cu Kα radiation (**1**·0.5C_4H_8O and **5**·0.5C_4H_8O). A set of 25 carefully centered reflections was used for the centering procedure of the crystals and for determining the lattice constants. As a general procedure, the intensity of three standard reflections were measured periodically every 2 h for orientation and intensity control. This procedure did not reveal an appreciable decay of intensities for **5**·0.5C_4H_8O, while a decay of about 5% was noticed for the specimen of **3**·C_4H_8O. A more significant decay was observed for **1**·0.5C_4H_8O so that two different crystals were used for the data collection of this compound. All of the data were corrected for Lorentz and polarization effects. Empirical correction for the absorption effect was performed at an advanced state of the structure refinement by using the program DIFABS.[20] Atomic scattering factors were those tabulated by Cromer and Waber[21] with anomalous dispersion corrections taken from ref 22. The computational work was performed on a Digital DEC 5000/200 computer (**1**·0.5C_4H_8O and **5**·0.5C_4H_8O) or an HP Vectra/486 computer by using the SHELX-76 program.[23] The programs PARST,[24] ORTEP[25] , ZORTEP,[26] and SIR92[27] were also used. Final atomic coordinates of all atoms and structure factors are available as Supporting Information.

[(PP$_3$)Fe(H)(η^2-H$_2$)]BPh$_4$·0.5C$_4$H$_8$O (1·0.5C$_4$H$_8$O). Pale yellow crystals of **1**·0.5C_4H_8O were grown by slow diffusion of ethanol into a diluted THF solution of **1** under a constant stream of hydrogen. The structure was solved by heavy atom and Fourier techniques and refined by full-matrix least-squares methods. Anisotropic thermal parameters were used only for Fe, P, B, and C atoms of the polyphosphine ligands. At an advanced stage of the refinement two intensities of 0.6 e$^-$/Å^3 at the two *cis* positions of the octahedron around iron were considered potential H atoms. Although sound spectroscopic evidence shows the presence of an H_2 molecule at the position *trans* to the unique P atom of the PP_3 ligand, the two H components could not be resolved. However, the refinement of the H_2 ligand as a single hydride was relatively successful. In fact, the observed behavior was very similar to that pertaining to the classical hydride ligand undoubtely present in the *cis* position. All of the phenyl rings were treated as rigid bodies

(20) Walker, N.; Stuart, D. *Acta Crystallogr.* **1965**, *31*, 104.
(21) Cromer, D.; Waber, J. *Acta Crystallogr.* **1983**, *39A*, 158.
(22) *International Tables of X-ray Crystallography*; Kynoch Press: Birmingham, U.K. 1974; Vol. 4.
(23) Sheldrick, G. M. *SHELX-76 Program for Crystal Structure Determination*; University of Cambridge: Cambridge, U.K., 1976.
(24) Nardelli, M. *Comput. Chem.* **1983**, *7*, 95.
(25) Johnson, C. K. *Report ORNL-5138;* Oak Ridge National Laboratory: Oak Ridge, TN, 1976.
(26) Zsolnai, L.; Pritzkow, H. *ZORTEP*, University of Heidelberg: Germany, 1994.
(27) Altomare, A.; Burla, M.; Camalli, G.; Cascarano, G.; Giacovazzo, C.; Guagliandi, A.; Polidori, G. *J. Appl. Crystallogr.* **1994**, *27*, 435.

Table 2. Selected Molecular Properties for H_2, C_2H_4, CO, and N_2: Binding Energies (BE), Bond Lengths (BL), Bond Angles (BA), Dipole Moments (μ), First Ionization Energy (IE), and Selected Vibrational Frequencies (ω_c)[a]

molecule	−BE[b] (eV)	BL (Å)	BA (deg)	μ[e] (D)	IE[f] (eV)	ω_c[g] (cm^{-1})
H_2	4.57 (4.49)[b]	0.766 (0.742)[c]	180	0	16.20 (15.43)	4179 (4401)
C_2H_4	26.52 (23.07)[b]	1.09 (1.09)[d] (C−H) 1.32 (1.34)[d] (C−C); 116.8 (117.8)[d] (HCH)		0	11.19 (10.51)	1407 (1443) $\nu_{12}(CH_2)$; 1664 (1623) ν_2(CC); 3062 (2990) ν_{11}(CH); 3167 (3106) ν_9(CH); 3143 (3272) ν_5(CH)
CO	12.84 (11.11)[b]	1.129 (1.128)[c]	180	0.217 (0.122)[h]	14.17 (14.00)	2159 (2169)
N_2	11.19 (9.76)[b]	1.098 (1.097)	180	0	16.08 (15.58)	2398 (2359)

[a] Experimental values in parentheses. [b] Reference 48. [c] Reference 43. [d] Reference 28b. [e] Reference 49. [f] Experimental IEs[50] are compared with Slater's Transition State IEs obtained (TSIE) by running spin−polarized calculations.[51] [g] Vibrational frequencies from references 43 and 52. [h] The computed CO electric dipole moment has the correct orientation (in the sense C^-O^+).

with D_{6h} symmetry (C−C = 1.39 Å), and the hydrogen atoms were introduced at calculated positions (C−H = 1.08 Å). The difference map also revealed the presence of a molecule of THF solvent which was attributed a population factor of 0.5. The final difference map was featureless.

[(PP$_3$)Ru(H)(η^2-H$_2$)]BPh$_4$·0.5C$_4$H$_8$O (5·0.5C$_4$H$_8$O). Pale yellow crystals of **5**·0.5C_4H_8O were grown by slow diffusion of ethanol into a diluted THF solution of **5** under a constant stream of hydrogen. The structure was solved by heavy atom and Fourier techniques and refined by full-matrix least-squares methods. Anisotropic thermal parameters were used only for Ru, P, B, and C atoms of the polyphosphine ligands. All of the phenyl rings were treated as rigid bodies with D_{6h} symmetry (C−C = 1.39 Å), and the hydrogen atoms were introduced at calculated positions (C−H = 1.08 Å). However, the hydride ligands, not located on ΔF maps, were not included in the model. The difference map also revealed the presence of a molecule of THF solvent which was attributed a population factor of 0.5.

[(PP$_3$)Fe(H)(CO)]BPh$_4$·C$_4$H$_8$O (3·C$_4$H$_8$O). A thin lemon yellow parallelepiped of **3**·C_4H_8O, suitable for an X-ray diffraction study, was slowly grown from a diluted THF solution of **3** layered with ethanol and kept under a positive pressure of argon. The structure was solved by direct methods using the SIR92 program[27] and all of the non-hydrogen atoms were located through a series of F_o Fourier maps. Refinement was done by full-matrix least-squares calculations, initially with isotropic thermal parameters, and then, during the least-squares refinement, Fe, P, and C atoms, except the carbonyl carbon atom, were allotted anisotropic thermal parameters. At the last stage of the refinement, an intensity of 0.85 $e^-/Å^3$, near the metal atom, was located in the difference map and successfully refined in the least-squares cycles as the hydride ligand, with free positional and isotropic thermal parameters. The difference map also revealed the presence of a molecule of THF solvent which was successfully retained in the model.

XPS Measurements. A Perkin-Elmer Φ 5600ci spectrometer with standard Mg Kα radiation (1253.6 eV) was used for the XPS analyses. The working pressure was less than 1.8×10^{-9} mbar. The spectrometer was calibrated by assuming the binding energy (BE) of the Au $4f_{7/2}$ line at 83.9 eV with respect to the Fermi level. As an internal reference for the peak positions the C 1s peak of hydrocarbon contamination has been assumed at 284.8 eV. The standard deviation in the BE values of the XPS lines is 0.10 eV. After a Shirley-type background subtraction, the raw spectra were fitted using a nonlinear least-squares fitting program adopting Gaussian−Lorentzian peak shapes for all of the peaks. The powder samples were pressed onto a grooved copper plate and immediately introduced into the analysis chamber. No flood gun was used to avoid sample charging, in order to minimize the possibility of sample decomposition due to the electron beam.

Computational Details. All calculations have been run by using the DMOL method,[28] an *ab initio* total energy numerical method where the local density functional (LDF) Kohn−Sham equations are solved for systems with a finite size providing energy eigenvalues, eigenvectors, and charge distribution and allowing the analytic evaluation of energy gradients (force calculations). Exact numerical LDF spherical-atom atomic orbitals (NAOs) are used as basis functions. Because of the quality of these orbitals, basis set superposition effects are minimized and a good description of even weak bonding interactions is possible.[28a] It has already been shown[29] that a double numerical basis set (DN), obtained by increasing the functions of the neutral atom by the atomic valence functions of the corresponding 2+ ions, provides good results and that DN bond lengths (BLs) and DN bond angles (BAs) in the geometry optimization of molecular systems usually converge within ∼0.01 Å and 1°, respectively. In order to ensure a sufficiently high variational flexibility, the following NAOs obtained from LDF calculations relative to free atoms/ions have been employed: (a) Ru, the 1s−5s NAOs of the neutral ruthenium atom, the 4d−5p NAOs of Ru^{2+}; (b) Fe, the 1s−4s NAOs of the neutral iron atom, the 3d−4p NAOs of Fe^{2+}; (c) P, the 1s−3p NAOs of the neutral phosphorus atom, the 3s−3d NAOs of P^{2+}; (d) O, the 1s−2p NAOs of the neutral oxygen atom, the 2s−2p NAOs of O^{2+} and two sets of 3d, 2p, and 1s NAOs generated from two hydrogenic calculations using $Z = 5$ and $Z = 7$; (e) N, the 1s−2p NAOs of the neutral nitrogen atom, the 2s−2p NAOs of N^{2+} and two sets of 3d, 2p, and 1s NAOs generated from two hydrogenic calculations using $Z = 5$ and $Z = 7$; (f) C, the 1s−2p NAOs of the neutral carbon atom, the 2s−2p NAOs of C^{2+} and two sets of 3d, 2p, and 1s NAOs generated from two hydrogenic calculations using $Z = 5$ and $Z = 7$; (g) H, the 1s NAO of the neutral hydrogen atom and two sets of 1s and 2p NAOs generated from two hydrogenic calculations using $Z = 1.3$ and $Z = 4$. During the calculations, the Ru 1s−3d NAOs, the Fe 1s−2p NAOs and the P, O, N, and C 1s NAOs have been kept frozen in a fully occupied configuration, allowing their exclusion from the variational space. Detailed information about the numerical integration scheme is reported in ref 28a. Here, it is sufficient to specify that a number ≤ 1000 sample points/atom has been used. The integration points are spherically distributed around each atomic site. Radial points are taken from the nucleus to an outer distance of 10 bohr. The number of radial points (N_R) in the selected range is designed to scale up with increasing atomic number (Z): $N_R = 14(Z + 2)^{1/3}$. As for the l value of the one−center expansion about each nucleus is concerned, a value of l one greater than that in the atomic basis set has been found to provide sufficient precision.[28a] Here, we have adopted the following degrees of angular truncation: $l = 3$ for Fe and Ru and $l = 2$ for P, O, N, C, and H. The use of sets (d) ÷ (g) for the subsequent free molecules C_2H_4, CO, N_2, and H_2 has been found to be adequate to correctly reproduce a series of molecular properties as bond lengths (BL), bond angles (BA), vibrational frequencies (ν), dipole moments (μ), and ionization energies (IEs) (Table 2).

As it is shown in ref 30, the main discrepancy between theory and experiment usually regards the molecular atomization energy (AE) which, on the other hand, is a well-known drawback of the local density approximation (LDA).[31] In ref 30, it was also pointed out that a definite improvement can be obtained by using the Becke 1988 version of a gradient corrected exchange functional.[32] Since our main interest in the present theoretical analysis was the electronic and molecular structure of the prototype molecular ions rather than their overall AEs, we have limited our investigation to the use of the LDA. All

(28) (a) Delley B. *J. Chem. Phys.* **1990**, *92*, 508. (b) Delley B. J. *Chem. Phys.* **1991**, *94*, 7245.

(29) (a) Casarin, M.; Tondello, E.; Vittadini, A. *Surf. Sci.* **1994**, *303*, 125, and references cited therein. (b) Casarin, M.; Tondello, E.; Vittadini, A. *Surf. Sci.* **1994**, *307/309*, 1182. (c) Casarin, M.; Tondello, E.; Vittadini, A. *Inorg. Chim. Acta* **1995**, *235*, 151.

(30) Casarin, M.; Favero, G.; Tondello E.; Vittadini A. *Surf. Sci.* **1994**, *317*, 422.

(31) Ziegler T. *Chem. Rev.* **1991**, *91*, 651.

(32) Becke, A. D. *J. Chem. Phys.* **1988**, *88*, 2547.

Scheme 1

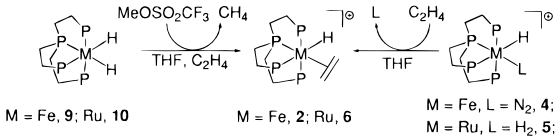

calculations have been performed on a workstation IBM 6000/550 at the Inorganic Chemistry Department of the University of Padova.

Results and Discussion

Synthesis and Spectroscopic Characterization of [(PP_3)-M(H)(η^2-C_2H_4)]BPh_4 (M = Fe, 2; Ru, 6). The reaction of $MeOSO_2CF_3$ with a THF solution of the dihydride complexes [$(PP_3)MH_2$] (M = Fe, **9**; Ru, **10**) under an atmosphere of ethene (Scheme 1) is an excellent method for the synthesis of the new octahedral *cis*-hydride−ethene complexes [(PP_3)M(H)(η^2-C_2H_4)]$^+$ (M = Fe, **2**; Ru, **6**) which can be isolated as tetraphenylborate salts upon addition of $NaBPh_4$. Alternatively, compounds **2** and **6** can be prepared by bubbling ethene into THF solutions of [(PP_3)M(H)(L)]BPh_4 complexes [M = Ru, L = N_2 (**8**), H_2 (**5**); M = Fe, L = N_2 (**4**)].

The two (hydride)ethene complexes **2** and **6** exhibit a totally different stability in solution. In particular, while the ruthenium derivative is air-stable and does not eliminate ethene under argon, dihydrogen, or dinitrogen, the iron derivative is air- and moisture-sensitive and readily decomposes to give the paramagnetic dark-violet five-coordinate derivative [(PP_3)FeH]BPh_4.[17] Moreover, the iron derivative readily undergoes in solution the displacement of ethene by carbon monoxide, dinitrogen, or dihydrogen to form the known [(PP_3)Fe(H)(L)]BPh_4 compounds (L = CO, N_2, and H_2),[1,16] whereas the ethene ligand in the Ru derivative **6** is displaced by CO to give the (hydride)carbonyl complex [(PP_3)Ru(H)(CO)]BPh_4 (**7**) but not by N_2 or H_2.[2]

The IR spectrum of the iron derivative does not display any absorption ascribable to a ν(Fe−H) vibration. In contrast, a weak band at 1972 cm^{-1} in the IR spectrum of **6** is assigned to ν(Ru−H). In keeping with an octahedral coordination geometry around the metal centers, both **2** and **6** exhibit an AMQ_2 splitting pattern in their $^{31}P\{^1H\}$ NMR spectra.[1,2,17,33] The high-field components in the spectrum of **6** are slightly perturbed by second-order effects. The Ru derivative is stereochemically rigid on the NMR time scale, while the iron complex features a dynamic behavior as shown by the broadening of the phosphorus resonances at room temperature. Unfortunately, the observation of the fast-exchange spectrum was not possible due to extensive decomposition of **2** in CD_4Cl_2/toluene-d_8 solution at temperatures higher than 40 °C. Above this temperature, a deep violet solution was invariably obtained with no signal detectable in the ^{31}P NMR spectrum over a spectral width of 100 000 Hz, which suggests the conversion to the above mentioned paramagnetic five-coordinate [(PP_3)FeH]$^+$ species. In contrast, the scrambling process which makes equivalent the terminal phosphorus nuclei of the PP_3 ligand, is frozen already at −25 °C. At this temperature, the ^1H NMR spectrum of **2** exhibits a high-field multiplet which is assigned to the terminal hydride ligand. Interestingly, this resonance appears as a doublet of triplets (δ_{FeH} −8.43, J_{HPM} = 63.4 Hz, J_{HPQ} = 47.7 Hz) with no apparent coupling to the *cis* disposed bridgehead phosphorus atom. This unique feature of the proton NMR spectrum of **2** is not observed in the spectrum of the ruthenium complex **6** where a canonical doublet of triplets of doublets centered at −8.85 ppm is displayed.[2,33] A broad signal (**2**, δ 3.43; **6**, δ 3.58) corresponding to four protons and featuring the shape of an unresolved quartet in the iron derivative ($J_{HPM} \approx J_{HPN}$ 3.0 Hz) is assigned to the four equivalent protons of the metal coordinated ethene molecule, which consistently should freely rotate about the M−C_2H_4 axis. This assignment is supported not only by the chemical shift values[34] but also by the results of a 2D-^1H,^{13}C-NMR HETCOR experiment for complex **6**. In fact, the $^{13}C\{^1H\}$ NMR spectrum of **6** contains a doublet of quartets at 51.69 ppm (J_{CPA} = 7.5 Hz, $J_{CPM} \approx J_{CPN}$ = 1.3 Hz) which inverts in a DEPT experiment and thus can unequivocally be assigned to the π-ethene carbon atoms. As a matter of fact, from an examination of the cross-peaks network (HMQC 2D-NMR experiment), one can correlate this carbon resonance with the broad singlet at 3.58 ppm. The low stability of **2** in all common NMR solvents did not allow us to record an informative ^{13}C NMR spectrum.

X-ray Diffraction Studies. X-ray diffraction analyses were carried out on the iron and the ruthenium dihydrogen−hydride complexes after recrystallization from THF/ethanol mixtures which gave the hemisolvate adducts **1**·0.5THF and **5**·0.5THF. An X-ray structure determination was undertaken also on the iron(II) (hydride)carbonyl complex **3** after the compound was recrystallized from THF/ethanol solution to give **3**·THF.

The crystal structure of the two nonclassical polyhydrides consists of discrete [$(PP_3)MH_3$]$^+$ cations (M = Fe, Ru), tetraphenylborate anions, and clathrated THF molecules in a 1:1:0.5 ratio. Selected bond lengths and angles are given in Table 3, while ORTEP drawings of the complex cations are presented in Figure 1 (Fe) and Figure 2 (Ru).

A stoichiometric ratio of 1:1:1 features the crystal structure of the carbonyl complex **3**·THF which contains [(PP_3)Fe(H)-(CO)]$^+$ cations, tetraphenylborate anions and interspersed THF solvent molecules in the lattice. A perspective view of the complex cation is shown in Figure 3, while selected metrical data are provided in Table 3.

All complex cations exhibit distorted octahedral structures with the (PP_3)M fragment adopting a pseudo C_{2v} symmetry. Indeed, distortions from the idealized octahedral geometry are invariably encountered in transition metal complexes of tripodal polyphosphines and are generally determined by the steric constraints imposed by this type of chelating ligands.[33]

In the present complexes, the largest deviation from the octahedral geometry is associated with the opening of the P(1)−M−P(2) angle which ranges from 153.0(2)° (**3**·THF) to 154.1(1)° (**1**·0.5THF). This kind of deformation is a common feature of six-coordinate PP_3 metal complexes irrespective of the transition metal.[33] Among the several structures which are relevant to this study, it is worth mentioning the nonclassical trihydride [$(PP_3)OsH_3$]BPh_4 (**11**) [157.0(1)°][35] and the iron derivative [(PP_3)Fe{η^2-*O*,*O*′-$O_2CCH_2CH_2C{\equiv}CH$}]BPh_4 [159.7-(1)°].[36] A still more relevant bending with respect to the ideal

(33) For other examples of octahedral complexes of PP_3 see: (a) Bianchini, C.; Masi, D.; Meli, A.; Peruzzini, M.; Zanobini, F. *J. Am. Chem. Soc.* **1988**, *110*, 6411. (b) Bianchini, C.; Meli, A.; Peruzzini, M.; Ramirez, J. A.; Vacca, A.; Vizza, F.; Zanobini, F. *Organometallics* **1989**, *8*, 337. (c) Bianchini, C.; Masi, D.; Meli, A.; Peruzzini, M.; Ramirez, J. A.; Vacca, A.; Zanobini, F. *Organometallics* **1989**, *8*, 2179. (d) Di Vaira, M.; Peruzzini, M.; Stoppioni, P. *Inorg. Chem.* **1991**, *30*, 1001. (e) Bianchini, C.; Linn, K.; Masi, D.; Mealli, C.; Peruzzini, M.; Zanobini, F. *Inorg. Chem.* **1992**, *31*, 4036. (f) Barbaro, P.; Bianchini, C.; Peruzzini, M.; Polo, A.; Zanobini, F. *Inorg. Chim. Acta* **1990**, *220*, 5. (g) Bianchini, C.; Frediani, P.; Masi, D.; Peruzzini, M.; Zanobini, F. *Organometallics* **1994**, *13*, 4616. (h) Jia, G.; Drouin, S.; Jessop, P. G.; Lough, A. J.; Morris, R. H. *Organometallics* **1993**, *12*, 906.

(34) See for example: (a) Werner, H.; Schwab, P.; Wolf, J. *Chem. Ber.* **1992**, *125*, 2641. (b) Barbaro, P.; Bianchini, C.; Meli, A.; Peruzzini, M.; Vacca, A.; Vizza, F. *Organometallics* **1991**, *10*, 2227.

(35) Bianchini, C.; Linn, K.; Masi, D.; Peruzzini, M.; Polo, A.; Vacca, A.; Zanobini, F. *Inorg. Chem.* **1993**, *32*, 2366.

Table 3. Selected Bond Distances (Å) and Angles (deg) for **1**·0.5THF, **3**·THF, and **5**·0.5THF

	1·0.5THF[a]	**3**·THF	**5**·0.5THF
Fe−P(1)	2.208(3)	2.222(3)	
Fe−P(2)	2.217(3)	2.216(3)	
Fe−P(3)	2.223(3)	2.236(4)	
Fe−P(4)	2.150(3)	2.181(4)	
Fe−H(1)	1.59(7)	1.44(10)	
Fe−H(2)	1.6(1)		
Ru−P(1)			2.350(3)
Ru−P(2)			2.334(4)
Ru−P(3)			2.369(3)
Ru−P(4)			2.249(3)
Fe−C(7)		1.69(1)	
C(7)−O(1)		1.17(2)	
P(1)−Fe−P(2)	154.1(1)	153.0(2)	
P(1)−Fe−P(3)	101.2(1)	107.7(2)	
P(1)−Fe−P(4)	86.0(1)	85.8(1)	
P(2)−Fe−P(3)	102.8(2)	103.8(2)	
P(2)−Fe−P(4)	85.6(1)	84.6(1)	
P(3)−Fe−P(4)	87.2(1)	86.6(1)	
H(1)−Fe−P(1)	92(3)	77(4)	
H(1)−Fe−P(2)	96(3)	76(3)	
H(1)−Fe−P(3)	96(3)	166(4)	
H(1)−Fe−P(4)	176(2)	80(4)	
H(2)−Fe−P(1)	83(3)		
H(2)−Fe−P(2)	72(3)		
H(2)−Fe−P(3)	167(4)		
H(2)−Fe−P(4)	81(4)		
H(1)−Fe−H(2)	96(4)		
H(1)−Fe−C(7)		95(4)	
Fe−C(7)−O		174(1)	
C(7)−Fe−P(1)		97.4(5)	
C(7)−Fe−P(2)		89.8(5)	
C(7)−Fe−P(3)		99.0(5)	
C(7)−Fe−P(4)		172.9(5)	
P(1)−Ru−P(2)			153.9(1)
P(1)−Ru−P(3)			100.3(1)
P(1)−Ru−P(4)			84.3(1)
P(2)−Ru−P(3)			99.1(1)
P(2)−Ru−P(4)			83.5(1)
P(3)−Ru−P(4)			84.5(1)

[a] In the (dihydrogen)hydride complex **1**·0.5THF, H(1) represents the two hydrogen atoms of the H_2 ligand. Crystallographically, the two H atoms appear as a unique unresolved peak and have been left out of the ORTEP diagram (Figure 1).

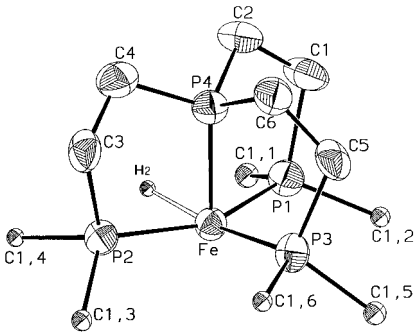

Figure 1. ORTEP drawing of the complex cation $[(PP_3)Fe(H)(\eta^2\text{-}H_2)]^+$. Only the *ipso* carbons of the phenyl rings are shown for the sake of clarity.

value of 180° has been found in the hydride−carbonyl complex $[(NP_3)Fe(H)(CO)]BPh_4$ (**12**) [142.1(1)°] [NP_3 = $N(CH_2CH_2PPh_2)_3$].[37]

In keeping with the molecular structure of **11**[35] as well as the spectroscopic characterization of **1**[1] and **5**,[2] a terminal

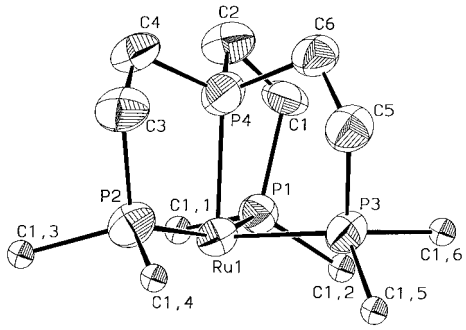

Figure 2. ORTEP drawing of the complex cation $[(PP_3)Ru(H)(\eta^2\text{-}H_2)]^+$. Only the *ipso* carbons of the phenyl rings are shown for the sake of clarity.

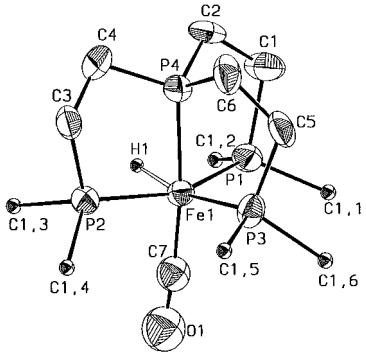

Figure 3. ORTEP drawing of the complex cation $[(PP_3)Fe(H)(CO)]^+$. Only the *ipso* carbons of the phenyl rings are shown for the sake of clarity.

hydride and a nonclassical H_2 ligand must be located mutually *cis* in the equatorial plane of the octahedron defined also by the bridgehead P_4 atom and by one terminal PPh_2 group (P_3). In the structure of **3**·THF, a terminal carbonyl ligand occupies the position *trans* to a bridgehead P_4 atom which is taken by the nonclassical ligand in both **1**·0.5THF and **5**·0.5THF. However, although the presence of the hydride ligands was apparent from the difference Fourier maps in both **1**·0.5THF and **5**·0.5THF, the refinement procedures were unsuccessful.[11,38] We could not precisely locate the hydride ligands in the structure of the ruthenium complex and could only approximate their position in the iron complex **1**·0.5THF. A similar situation was encountered in the structure of **11**,[35] where a single unresolved electron density *trans* to the bridgehead P_4 atom in the Fourier difference map was treated as a single hydride (H(1) in Table 3), although there is a clearcut spectroscopic evidence pointing to presence of a molecular hydrogen ligand in this position.[1,2]

The Fe−H bond distances found in the polyhydride **1**·0.5THF are similar to each other [1.59(7) *vs* 1.6(1) Å] and falls within the range reported by Orpen and co-workers [$d_{Fe-H_{av}}$ = 1.609 Å, σ = 0.004].[39] A similar relationship between the Os−H and Os−H_2 bond lengths has already been observed in **11**. Interestingly, the Fe−H bond distance in the hydride−carbonyl complex **3**·THF [1.44(10) Å] is significantly shorter than those pertaining to the classical and nonclassical hydrides in **1**·0.5THF, but matches well with the value reported for the hydride−carbonyl complex **12** [1.43(9) Å].[37]

In agreement with the strong *trans* influence exerted by the terminal hydride ligand, the P_3 atom *trans* to the hydride exhibits the longest M−P separation.[33,35] The other Fe−P and Ru−P bond distances are within the range found for other phosphine

(36) Linn, K.; Masi, D.; Mealli, C.; Bianchini, C.; Peruzzini, M. *Acta Crystallogr.* **1992**, *C48*, 2220.
(37) George, T. A.; Rose, D. J.; Chang, Y.; Chen, Q.; Zubieta, J. *Inorg. Chem.* **1995**, *34*, 1295.
(38) Bau, R.; Teller, R. G.; Kirtley, S. W.; Koetzle, T. F. *Acc. Chem. Res.* **1979**, *12*, 176.
(39) Orpen, A. G.; Brammer, L.; Allen, F. H.; Kennard, O.; Watson, D. G.; Taylor, R. *J. Chem. Soc., Dalton Trans.* **1989**, S1.

Table 4. Binding Energy Values (eV) for $[(PP_3)Fe(H)(L)]BPh_4$ (L = H_2, **1**; C_2H_4, **2**; CO, **3**; N_2, **4**)

compound	Fe $2p_{3/2}$	P 2p
$[(PP_3)Fe(H)(\eta^2\text{-}H_2)]BPh_4$	708.2	131.5
$[(PP_3)Fe(H)(\eta^2\text{-}C_2H_4)]BPh_4$	708.4	131.7
$[(PP_3)Fe(H)(CO)]BPh_4$	709.1	131.8
$[(PP_3)Fe(H)(\eta^1\text{-}N_2)]BPh_4$	708.4	131.7

complexes of iron(II)[36,40] and ruthenium(II)[33e,g] stabilized by tripodal polyphosphine ligands.

XPS Measurements. Table 4 reports the binding energies of Fe $2p_{3/2}$ and P 2p peaks for complexes **1**−**4**. As expected for polyphosphine organometallic compounds, the values of the binding energies are significantly different from those of molecular systems where a d^6 metal ion is coordinated by "hard" ligands such as O, N, or Cl and has a formal oxidation number of +2.[41] Actually, the lower binding energies we have measured are consistent with an oxidation state closer to 0 or +1. Such a difference is attributed to the large number of phosphine donor atoms which increase the electron density around the metal center.

Comparable binding energy values of the Fe $2p_{3/2}$ peak have been found for compounds **1**, **2,** and **4** (Table 4), whereas this peak lies at significantly higher binding energy in **3.** The observed trend of binding energies can be related to the different contribution of back-donation from occupied Fe 3d t_{2g}-like levels (despite the absence of any symmetry element in the structure of the prototype molecular ions, it is still possible to pick up the e_g and t_{2g} character of Fe 3d based AOs) into the virtual levels of the sixth ligand L (L = H_2, C_2H_4, CO, N_2), and points out that this interaction is very strong when L = CO.

A further point to consider is that the Fe $2p_{3/2}$ band shape of the carbonyl complex **3** is different from those observed for **1**, **2**, or **4**. There is, in fact, a strong shake up of the structure, indicating that final state effects cannot be neglected in the photoionization process. Therefore, simple considerations based on the electron density calculated on the metal may lead to wrong previsions about the binding energy values.

XPS data are not reported for the Ru complexes as the Ru 3d peak extensively overlaps with the very intense C 1s peak; the binding energies thus cannot precisely be determined.

Theoretical Results. Ball and stick representations of the complex cations $[\{P(CH_2CH_2PH_2)_3\}Fe(H)(H_2)]^+$ (L = H_2, **1***; C_2H_4, **2***; CO, **3***; N_2, **4***) are reported in Figure 4 ($[\{P(CH_2\text{-}CH_2PH_2)_3\}Ru(H)(H_2)]^+$, **5***, is isostructural with **1***). Unlike the carbonyl **3** and dinitrogen **4** derivatives, two conformers are possible for the dihydrogen and ethene complexes **1** and **2**: one with the L ligand parallel (∥) to the M−H_i bond (H_i = terminal hydride), the other with L perpendicular (⊥) to it. Both conformations have been taken into account for the Fe complexes **1*** and **2***, while only the H_2 derivative **5*** has been investigated for Ru.

From a perusal of Table 5, one may readily infer that only slight variations of the geometrical parameters are exhibited by the $[\{P(CH_2CH_2PPH_2)_3\}Fe(H)]^+$ fragment along the investigated series, which is in good agreement with crystallographic data for **1** and **3**. An analogous agreement is obtained for $\mathbf{5}^*_{\parallel}$ and $\mathbf{5}^*_{\perp}$ (Table 6). The largest deviation between theory and experiment has systematically been found for the M−P_e distances as a consequence of the substitution of the actual phenyl groups with hydrogen atoms. Consistently, the agreement between experimental and theoretical Fe−P_a bond lengths is much better.

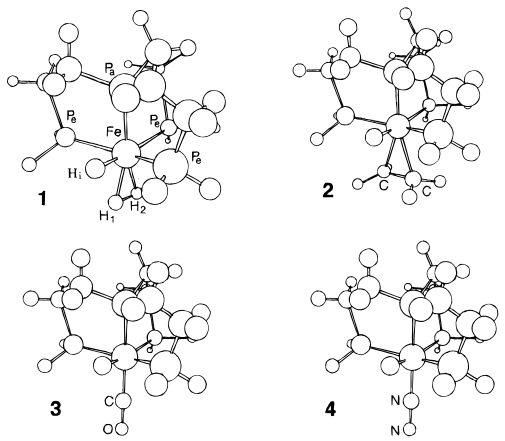

Figure 4. Ball and stick representations of the complex cations $[\{P(CH_2CH_2PH_2)_3\}Fe(H)(L)]^+$ (L = H_2, **1***; C_2H_4, **2***; CO, **3***; N_2, **4***).

Selected gross atomic charges (*Q*) and overlap populations (OPs) obtained from the Mulliken[42] population analysis are reported in Tables 7 and 8. An inspection of these tables clearly indicates that the metal center carries a significant amount of electronic charge as a consequence of the strong donation from the P lone pairs (it is worth mentioning that the overall positive charge carried by the complex cations is almost completely localized over the H atoms of the model PH_2 groups). In agreement with the XPS measurements (Table 4), the negative charge localized over the Fe atom in **1*** is the largest in the series, most probably due to the weak back-donation from the occupied 3d Fe t_{2g}−like AOs (d_{xy}, d_{xz}, d_{yz} in our framework) into the high-lying H_2 σ^* MO. The poor back-donation into the σ^* H_2 level is thus consistent with the presence of an intact H_2 ligand, although we observe a significant decrease of the H−H OP upon H_2 coordination (Table 7). Most importantly, the total energy corresponding to the optimized molecular structure of $\mathbf{1}^*_{\parallel}$ is lower than that of $\mathbf{1}^*_{\perp}$ by about 1.5 kcal mol^{-1} (a rotational barrier of 1.82 kcal mol^{-1} was determined for the H_2 ligand by the INS studies).[8] A reasonable explanation of the higher stability of $\mathbf{1}_{\parallel}$ is offered by the weak but not negligible bonding interaction between H_i and H_2 (OP = 0.047e). As a whole, the present results are in excellent agreement with those obtained by Bertrán and co-workers for the model compound *cis*-$[Fe(PH_3)_4(H)(H_2)]^+$.[14,15] Also in this model system, the conformer where the H_2 ligand is placed in the P−Fe−H plane (parallel orientation) is more stable than the perpendicular isomer. More importantly, the Fe−H_2 bond is much stronger in the parallel isomer and is also asymmetric due to an attractive cis effect between the terminal hydride and the H_2 ligand. The cis effect is suggested to be the factor which stabilizes the parallel isomer.[13] Different bonding distances between the metal center and the hydrogens of the H_2 ligand have experimentally been found in $Fe(H)_2(H_2)(PEtPh_2)_3$ authenticated by neutron diffraction.[13d] In the present theoretical analysis, we do not find asymmetry in the Fe−η^2-H_2 moiety (Table 5), most likely due to the limitations of the applied methodology, and the only evidence for the *cis* effect is provided by the bonding interaction between the terminal hydride H_i and one of the hydrogens of H_2. On the other hand, the existence of a cis effect is supported by the low-energy intramolecular exchange between the hydride and the molecular hydrogen in **1** [$\Delta G^{\ddagger}$(300 K) = 12 ± 1 kcal mol^{-1}].[1,11a] This exchange has been interpreted on both experimental[1,2] and theoretical grounds[15] as occurring through

(40) Bianchini, C.; Laschi, F.; Masi, D.; Ottaviani, F. M.; Pastor, A.; Peruzzini, M.; Zanello, P.; Zanobini, F. *J. Am. Chem. Soc.* **1993**, *115*, 2723.

(41) Siedle, A. R.; Newmark, R. A.; Korba, G. A.; Pignolet, L. H.; Boyle, P. D. *Inorg. Chem.* **1988**, *27*, 1593.

(42) Mulliken, R. S. *J. Chem. Phys.* **1955**, *23*, 1833.

Table 5. Selected Bond Lengths (BL) for **1***$_{||}$, **1***$_{\perp}$, **2***$_{||}$, **2***$_{\perp}$, **3***, and **4*** (When Available Experimental Values Are Given in Parentheses)[a]

1*			**2***			**3***		**4***	
	BL (Å)			BL (Å)			BL (Å)		BL (Å)
	1*$_{||}$	**1***$_{\perp}$		**2***$_{||}$	**2***$_{\perp}$				
$Fe-H_1$	1.56 (1.6)	1.57	$Fe-C_1$	2.06	2.06	Fe−C	1.75 (1.69)	Fe−N	1.80
$Fe-H_2$	1.56 (1.6)	1.57	$Fe-C_2$	2.07	2.08	C−O	1.15 (1.17)	N−N	1.11
$Fe-H_i$	1.51 (1.59)	1.51	$Fe-H_i$	1.49	1.52	$Fe-H_i$	1.51 (1.44)	$Fe-H_i$	1.51
H_2-H_1	0.95	0.93	C_2-C_1	1.39	1.40				
			$C-H(C_2H_4)$	1.09	1.10				
$Fe-P_a$	2.14 (2.15)	2.13 (2.15)		2.16	2.14		2.17 (2.18)		2.15
$Fe-P_e$[b]	2.15 (2.22)	2.15 (2.22)		2.15	2.14		2.14 (2.23)		2.16
P_a-C[b]	1.84 (1.82)	1.84 (1.82)		1.84	1.83		1.83 (1.82)		1.83
P_e-C[b]	1.85 (1.85)	1.85 (1.85)		1.84	1.83		1.84 (1.84)		1.84

[a] Key: P_a denotes the bridgehead phosphorus atom of PP_3 and P_e indicates the equatorial phosphorus atoms of PP_3; H_i denotes the terminal hydride ligand. [b] Mean value.

Table 6. Selected Bond Lengths (BL) for **5***$_{||}$ and **5***$_{\perp}$ (Experimental Values When Available Are Given in Parentheses)[a]

	BL (Å)			BL (Å)	
	5*$_{||}$	**5***$_{\perp}$		**5***$_{||}$	**5***$_{\perp}$
$Ru-H_1$	1.77	1.74	$Ru-P_a$	2.26 (2.25)	2.28 (2.25)
$Ru-H_2$	1.77	1.75	$Ru-P_e$[b]	2.31 (2.35)	2.31 (2.35)
$Ru-H_i$	1.63	1.64	P_a-C[b]	1.83 (1.84)	1.84 (1.84)
H_2-H_1	0.89	0.91	P_e-C[b]	1.85 (1.86)	1.85 (1.86)

[a] Key: P_a denotes the bridgehead phosphorus atom of PP_3 and P_e indicates the equatorial phosphorus atoms of PP_3; H_i denotes the terminal hydride ligand. [b] Mean value.

an open direct transfer mechanism. In particular, Jackson and Eisenstein have proposed that the nascent bond between the H and H_2 ligands is a factor that might lower the activation energy of intramolecular H exchange.[13a]

As in the isostructural Fe complex **1***, the total energy corresponding to the optimized molecular structure of the η^2-H_2 Ru derivative **5***$_{||}$ is more negative by 1.5 kcal mol^{-1} than **5***$_{\perp}$ (INS studies give a value of 1.36 kcal mol^{-1} for the barrier to rotation of the H_2 ligand).[8] The origin of such a ΔE is probably the same proposed for **1*** as we still observe an appreciable, even though smaller, bonding interaction between H_i and H_2 (OP = 0.032e) in the Ru complex. Within this context, it may be a useful reminder to mention that the main difference between the electronic structures of **1*** and **5*** is the stronger $Fe-H_2$ interaction in the former complex. Actually, the $Fe-H_2$ OP is dramatically larger than the $Ru-H_2$ one. Furthermore, the $M-H_2$ distance is definitely shorter in **1*** than in **5***. Bertrán and co-workers suggest that the origin of the interaction between the *cis* hydride and dihydrogen ligands is electrostatic in nature (due to the negative and positive charges supported by the H and H_2 ligands, respectively).[14,15] In this picture, the higher electronegativity of Ru as compared to Fe, decreasing the negative charge on the terminal hydride, would actually reduce the *cis* effect and ultimately account for the weaker $Ru-H_2$ bond as well as the slightly higher energy barrier to the H/H_2 exchange determined by NMR spectroscopy for **5** [$\Delta G^{\ddagger}$(300 K) = 13 ± 1 kcal mol^{-1}].[2,11a]

From the analysis of the theoretical data pertaining to the ethene complex **2*,** one may readily infer that (i) unlike the η^2-H_2 derivative **1***, the parallel conformer results less stable than the perpendicular one by *ca.* 4.5 kcal mol^{-1}, most likely due to steric hindrance; and (ii) independent of the assumed conformation, there is a relevant decrease of the C_1-C_2 OP in going from the free ligand to the coordinated one (Table 7). Further insight into the nature of the $Fe-C_2H_4$ interaction can be obtained by considering the OPs between the Fe 3d and $2p_z$ AOs of C_1 and C_2. The Fe 3d t_{2g}-like orbitals participate much more (0.065e (⊥); 0.069e (||)) than the Fe 3d e_g-like ones (0.032e (⊥); 0.033e (||)) to the $Fe-C_2H_4$ bonding, clearly showing that back-donation, if on the one hand it plays a leading role in the $Fe-C_2H_4$ interaction, on the other hand is the main origin of the C_1-C_2 bond weakening.

Unlike the C_1-C_2 OP in **2***, the C−O one in **3*** increases upon coordination (Table 7). Nevertheless, the C−O stretching frequency decreases in going from the free ligand (2143 cm^{-1})[43] to the coordinated one (1927 cm^{-1}). Such a variation of the C−O stretching frequency upon coordination perfectly matches our theoretical outcomes which give the values of 2159 and 2044 cm^{-1} for ν(C−O) in the free and coordinated molecules, respectively. These results are also in accord with those obtained for CO chemisorbed on CuCl,[44] confirming that between donation and back-donation interactions, the latter influences the C−O stretching frequency much more than the former. In the present case the C−O σ (π) OP moves from 0.054e (0.436e) to 0.254e (0.399e) upon coordination. The increase of the σ OP is rather close to that computed for CO on CuCl (0.200e *vs* 0.189e),[44] while the decrease of the π OP is twice as large as that computed for CO on CuCl (−0.037e *vs* −0.018e).[44] Accordingly, the red shift of the CO stretching frequency in **3** is significantly larger than that of CO chemisorbed on CuCl.[44] Interestingly, the red shift measured for ν(CO) in the iron derivative **2** ($\Delta\nu$ = 216 cm^{-1}) is larger than that of the Ru analog $[(PP_3)RuH(CO)]BPh_4$[2] ($\Delta\nu$ = 161 cm^{-1}). In a sense, this finding confirms that, in the present family of complexes, iron is better suited than ruthenium for π-back-bonding interactions. In contrast, steric effects might control the relative stability of ethene complexes **2** and **6,** which increases in the order Fe < Ru. Due to its smaller size, iron penetrates the cavity of the tripodal ligand more deeply than ruthenium and thus any bonding interaction with molecules of a certain size may be stereochemically disfavored (indeed, ethene is the only alkene that coordinates the metal center in the $[(PP_3)Fe(H)]^+$ system).[45]

As for the dinitrogen complex **4***, it is noteworthy that, despite a rather large Fe−N OP (indicative of a quite strong interaction between the metal center and the dinitrogen ligand), the N−N OP is substantially unaffected upon coordination. Two factors can concur to determine this finding: (i) the poor M → N_2 back-donation; (ii) the nonbonding character of the N_2-based $2\sigma_u$ MO that is responsible of the N_2 → M donation.

In conclusion, the experimental and theoretical observation that the Fe → L back-bonding interaction in the carbonyl

(43) Huber, K. P.; Herzberg, G. *Molecular Spectra and Molecular Structures. Constants of Diatomic Molecules*, Van Nostrand: New York, 1979; Vol. 4.
(44) Casarin, M.; Favero, G.; Tondello, E.; Vittadini, A. *Surf. Sci.* **1994**, *317*, 422.
(45) Bianchini, C.; Peruzzini, M. Unpublished results.

Table 7

(A) Effective Atomic Charges for **1***$_{\parallel}$, **1***$_{\perp}$, **2***$_{\parallel}$, **2***$_{\perp}$, **3*** and **4*** from Mulliken Population Analysis

	Fe	P_a	P_e	H_i	H_1	H_2	C_1	C_2	C	O	N_1	N_2
1*$_{\parallel}$	−0.72	0.11	−0.19	0.06	0.13	0.10						
1*$_{\perp}$	−0.72	0.10	−0.20	0.09	0.12	0.11						
2*$_{\parallel}$	−0.53	0.11	−0.19	0.08			−0.08	−0.18				
2*$_{\perp}$	−0.52	0.10	−0.17	0.06			-0.26	−0.19				
3*	−0.58	0.10	−0.20	0.08					0.23	−0.18		
4*	−0.48	0.10	−0.21	0.07							0.06	−0.07
C_2H_4							−0.10	−0.10				
CO									0.05	−0.05		

(B) Selected Overlap Populations (e × 10^{-3}) for **1***$_{\parallel}$, **1***$_{\perp}$, **2***$_{\parallel}$, **2***$_{\perp}$, **3***, and **4***

	Fe−H_1	Fe−H_2	H_2−H_1	Fe−C_1	Fe−C_2	C_2−C_1	Fe−C	C−O	Fe−N_1	N_1−N_2
1*$_{\parallel}$	164	167	132							
1*$_{\perp}$	155	164	133							
2*$_{\parallel}$				130	145	423				
2*$_{\perp}$				117	125	418				
3*							372	653		
4*									273	541
H_{2free}			419							
C_2H_{4free}						716				
CO_{free}								490		
N_{2free}										545

Table 8

(A) Effective Atomic Charges for **5***$_{\parallel}$ and **5***$_{\perp}$ from Mulliken Populations Analysis

	Ru	P_a	P_e	H_i	H_1	H_2
5*$_{\parallel}$	−0.61	0.10	−0.23	0.03	0.11	0.08
5*$_{\perp}$	−0.60	0.10	−0.24	0.04	0.10	0.109

(B) Selected Overlap Populations (e × 10^{-3}) for **5***$_{\parallel}$ for **5***$_{\perp}$

	Ru−H_1	Ru−H_2	H_2−H_1
5*$_{\parallel}$	115	98	200
5*$_{\perp}$	114	103	202

complex is much more efficient than those in the H_2, N_2, and C_2H_4 derivatives **1, 2**, and **4**, confirms that the relative stability of these four complexes is not exclusively dictated by π-back-donation, and suggests that an important role may be played by the *cis* effect operative only when L is H_2.

Conclusions

An *ab initio* study on the model systems [{$P(CH_2CH_2PH_2)_3$}-M(H)(L)]$^+$ (M = Fe, L = H_2, C_2H_4, CO, N_2; M = Ru, L = H_2), X-ray analyses, and XPS and NMR measurements on actual complexes with the tripodal tetraphosphine PP_3, taken altogether, have confirmed the peculiar effects of the hydride ligand on the bonding between a *cis* H_2 ligand and the metal center.

Though conclusive evidence accounting for the extrastability of the (dihydrogen)hydride Fe complex has not been obtained, both the theoretical and experimental studies are consistent with greater d(metal) → σ^*(H−H) back-donation and *cis* effect in the Fe complex as compared to the Ru analog. Other factors that may account for the stability of the Fe complex toward H_2 displacement by N_2, such as the different entropy of binding of H_2 *vs* N_2[46] or weaker Fe−P bond strengths, which would favor the decoordination of a phosphine arm of PP_3 over H_2 elimination, can safely be ruled out. The Fe−P bond distances in **1** fall in the usual range for iron−phosphine complexes and are even shorter than those determined in [Fe(η^2-H_2)H(Ph_2PCH_2-$CH_2PPh_2)_2$]BPh_4 which readily undergoes the displacement of H_2 by N_2.[47] Similarly, entropy arguments alone do not justify the stability of the dihydrogen−hydride Fe complex under a nitrogen atmosphere as they should equally affect the chemistry of the Ru complex.

Acknowledgment. We thank Mr. Febrizio Zanobini for his technical assistance.

Supporting Information Available: Tables of crystallographic data for **1**·0.5THF, **3**·THF, and **5**·0.5THF and of final positional parameters and isotropic and anisotropic displacement parameters for all atoms for **1**·0.5THF, **3**·THF, and **5**·0.5THF (17 pages). Ordering information is given on any current masthead page.

IC960736Q

(46) Gonzales, A. A.; Hoff, C. D. *Inorg. Chem.* **1989**, *28*, 4295.
(47) Ricci, J. S.; Koetzle, T. F.; Bautista, M. T.; Hofstede, T. M.; Morris, R. H.; Sawyer, J. F. *J. Am. Chem. Soc.* **1989**, *111*, 8823.
(48) Seminario, J. M. *Chem. Phys. Lett.* **1993**, *206*, 547.
(49) *CRC Handbook of Chemistry and Physics*, 64th ed.; CRC Press: Boca Raton, FL, 1984; p E−92.
(50) Rabalais, J. W. *Principles of Ultraviolet Photoelectron Spectroscopy*; J. Wiley Interscience: New York, 1977.
(51) Slater, J. C. *Quantum Theory of Molecules and Solids. The Self-Consistent Field For Molecules and Solids*; McGraw-Hill: New York, 1974; Vol. 4.
(52) Herzberg, G. *Infrared and Raman Spectra*; Van Nostrand: New York, 1945, p 173.